# Mechanism and Origin of Remote Stereocontrol in the Organocatalytic C(sp$^2$)-H Alkylation using Nitroalkanes as Alkylating Agents

Sharath Chandra Mallojjala,[a]‡ Rahul Sarkar,[b]‡ Rachael W. Karugu, [a] Madhu Sudan Manna, [b] Santanu Mukherjee,*[b]  and Jennifer S. Hirschi*[a]

**ABSTRACT:** Experimental 13C kinetic isotope effects (KIEs) and DFT calculations are used to evaluate the mechanism and the origin of enantioselectivity in the C(sp2)–H alkylative desymmetrization of cyclopentene-1,3-diones using nitroalkanes as the alkylating agent. An unusual combination of an inverse (~0.980) and a normal (~1.030) KIE is observed on the bond-forming carbon atoms of the cyclopentene-1,3-dione and nitroalkane, respectively. These data provide strong support for a mechanism involving reversible carbon-carbon bond-formation followed by rate- and enantioselectivity-determining nitro-group elimination. The theoretical free energy profile and predicted KIEs indicate that this elimination event occurs via an E1cB pathway. The origin of remote stereocontrol is evaluated by distortion-interaction and SAPT0 analyses of the enantio-meric E1cB transition states.
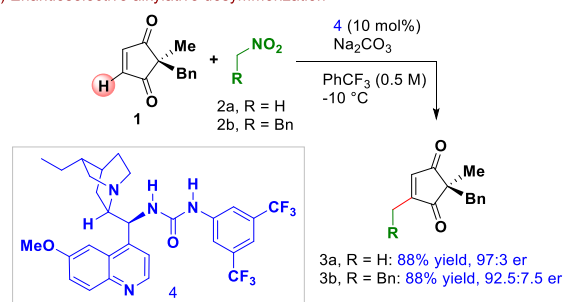
## Introduction

Direct functionalization of a specific C–H bond from a diverse ensemble of C–H bonds present in an organic molecule is arguably the most efficient and economic route for generating molecular complexity. The past decade has witnessed tremendous growth in the area of transition metal-catalyzed direct C–H activation,[1-3] mostly with the help of strategically placed directing groups. These approaches have often led to site selectivities unthinkable using conventional chemistry. Despite continuing developments of transition metal-catalyzed C–H activation reactions, functionalization of olefinic C(sp$^2$)–H bonds appears to be far more challenging when compared to aromatic C(sp$^2$)–H bonds. Moreover, introduction of an unfunctionalized alkyl group (e.g. methyl) into a specific C(sp$^2$)–H bond remains elusive. An additional level of difficulty arises when the C–H bond functionalization in question results in the generation of a stereocenter and the issue of enantiocontrol.

In 2015, one of our groups developed a simple strategy[4] for direct introduction of unfunctionalized alkyl groups into olefinic C(sp$^2$)–H bonds, not only enantioselectively but also without using directing group. This transformation utilizes air-stable and inexpensive nitroalkanes (**2**) as the alkyl source under the influence of a bifunctional tertiary amino-urea derivative (**4**) as the catalyst (Scheme 1A). More specifically, prochiral 2,2-disubstituted cyclopentene-1,3-diones (**1**) were desymmetrized enantioselectively through C(sp$^2$)–H alkylation. The generality of this strategy was subsequently demonstrated for the enantioselective desymmetrization of *meso*-norbornenoquinones. These transformations do not lead to the creation of any stereocenter at the reaction site but allow for the generation of stereocenter(s) remote from the reaction site – a phenomenon often termed as remote stereocontrol.
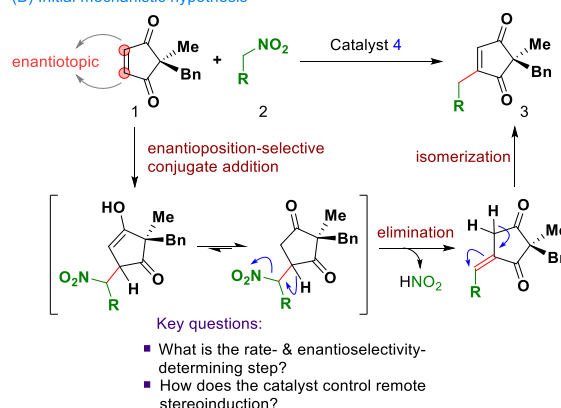
While the initial findings have already led to the development of other transformations and can be applied to the enantioselective synthesis of complex targets, a detailed mechanistic study of this reaction holds the potential to unearth valuable information.



**Scheme 1.** (A) Bifunctional chiral urea catalyzed enantioselective alkylative desymmetrization via formal sp$^2$ C-H functionalization.[4] (B) Originally proposed pathway and outstanding mechanistic questions addressed in this study.

As a preliminary hypothesis, an enantioposition-selective conjugate addition step of **2** to **1** was proposed to form the initial carbon–carbon bond. Elimination of the nitro group from this initial adduct followed by isomerization

presumably leads to formation of the desymmetrized product **3** (Scheme 1B). This addition-elimination-isomerization sequence likely occurs in the chiral pocket of the cinchona-alkaloid derived urea catalyst **4**. However, it is not immediately obvious which of the above steps is responsible for the origin of enantioselectivity observed in this reaction. Identification of the first irreversible step in the catalytic cycle is critical to obtain insights into how this bifunctional chiral urea orchestrates remote stereocontrol in this reaction.

In the modern era, density functional theory (DFT) calculations are widely employed in elucidating reaction mechanisms. On the other hand, DFT calculations in combination with the relevant experimental data have proven to be an even more powerful tool.[5-7]

In the present study, we utilize a combination of experimental ^{13}C kinetic isotope effects (KIEs) and density functional theory (DFT) calculations to probe the rate- and enantioselectivity determining step of the enantioselective C(sp[2])–H alkylation reaction described above.

## Results and Discussion

We chose the reaction of **1** with either **2a** or **2b** catalyzed by **4** for the determination of ^{13}C KIEs at natural abundance. The reaction between **1** and **2b** was used for the determination of intermolecular ^{13}C KIEs[8] by starting material analysis. Accordingly, two independent reactions of **1** and **2b** were taken to 65±2% and 64±2% conversion (in **2b**), and the unreacted **2b** was reisolated for the determination of ^{13}C KIEs. A large normal ^{13}C KIE of ~1.030 (Figure 1A) was observed on the carbon atom of **2b** bearing the nitro group. This is consistent with either C–C bond-formation or the nitro group elimination as the rate-determining step (RDS).[9]
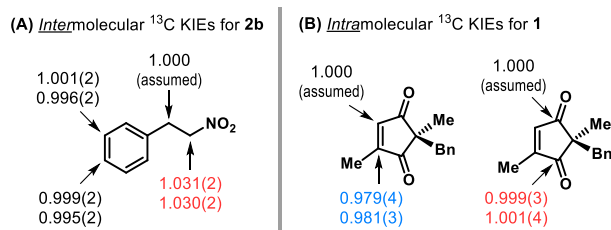


**Figure 1.** (A) Intermolecular 13C KIEs[8] determined for 2b. (B) Intra-molecular 13C KIEs[10] determined for 1. Two sets of KIEs represent independent experiments with six measurements per experiment. Numbers in parentheses show the uncertainty in last digit of each measurement.

Experimental KIEs for the enedione **1** were measured using intramolecular KIE methodology.[7,10] The intramolecular KIE for the first step that irreversibly desymmetrizes **1** in the catalytic cycle is determined by the relative ^{13}C integration in the NMR spectra of the desymmetrized product **3a**. A significant *inverse* [13]C KIE of ~0.980 was measured on the bond-forming carbon atom of **1** (Figure 1B). Qualitatively, these results rule out conjugate addition of **2a** to **1** as the first irreversible step in the catalytic cycle – since this would result in a significant *normal* KIE. Inverse ^{13}C KIEs are typically associated with increased steric crowding at a carbon center. This suggests that one of the steps after the C–C bond-formation is the first irreversible step in the catalytic

cycle for **1**. Since KIEs for **1** preclude the irreversible C–C bond-formation, nitro group elimination emerges as the most likely possibility for the rate- and enantioselectivity determining step in the catalytic cycle.

To aid in the quantitative interpretation of the experimental KIEs, a density functional theory (DFT) study was performed. A thorough potential energy surface scan on all reactants and catalysts was implemented to map the conformational and configurational space for this reaction. B3LYP[11] and B97-D[12-13] (with density fitting) functionals with a def2-SVP basis set[14] and polarized continuum model (IEFPCM)[15-16] were used for geometry optimization and for locating transition structures (TSs). Thermal corrections were calculated using Grimme's quasi-rigid rotor harmonic oscillator approximation.[17] The ^{13}C KIEs were calculated from the scaled vibrational frequencies using the method of Bigeleisen and Mayer[18] as implemented in Isoeff[19] and a Wigner tunneling correction[20] applied. Single point energies were calculated at M06-2X/6-311+G(d, p)[21,22] using Gaussian 16.[23] Interaction energies were calculated using SAPT0/jun-cc-pVDZ[24-27] as implemented in psi4.[28]

*Evaluation of key steps in the reaction coordinate*: The reaction is initiated by deprotonation of **2a** resulting in a protonated catalyst-nitronate complex. The lowest energy TS for this step (Figure 2A, **TS$_{deprot}$**) is stabilized by strong H-bonding interactions of the urea NHs with an oxygen of the nitro group while the acidic proton of the aci-nitro is deprotonated by the quinuclidine moiety of **4**. The ΔG‡ for **TS$_{deprot}$** is 12.6 kcal/mol relative to separated starting materials. Deprotonation is followed by the conjugate addition of this nitronate nucleophile to **1**, and the lowest energy TS for this step leads to the major enantiomer of product (**TS$_{add-R}$** , Figure 2A). The enedione **1** is bound via two strong H-bonding interactions to the two urea NHs (2.11 Å and 1.80 Å) and suffers attack by the nitronate, which is bound to the protonated quinuclidine via a strong H-bonding interaction (1.76 Å). The forming C–C bond distance in **TS$_{add-R}$** is 2.19 Å and this TS has a ΔG‡ of 18.5 kcal/mol (Figure 2B).

Next, we turned our attention to the mechanism of the nitro-elimination step, the likely rate- and enantioselectivity-determining step based on the qualitative interpretation of our experimental KIEs. A More O'Ferrall Jencks plot (Figure 2B) outlines the three possible mechanisms for nitro elimination from **Int 2** following **TS$_{add-R}$**. A detailed investigation of the E1 and E2 pathways revealed that these were prohibitively high in energy (ΔG‡ of 72.1 and 70.2 kcal/mol, respectively) and therefore not likely involved in the nitro-elimination from **Int 2** (See Supporting Information for detailed discussion). The E1cB mechanism can presumably be initiated by a catalyst mediated proton transfer from **Int 2** to form conjugate base **Int 2$_{cB}$**, which is protonated at the oxygen of the nitro-group, making it a good leaving group. Elimination of the protonated nitro-group from **int 2$_{cB}$** (**TS$_{E1cB-R}$**) has a ΔG‡ of 22.0 kcal/mol,[29] and represents the most likely pathway for the nitro-group elimination. The intermediate resulting from nitro group elimination (**Int 3**) is protonated via **TS$_{prot-R}$** (ΔG‡ = 18.3 kcal/mol) to deliver product **3a** and regenerate the catalyst.
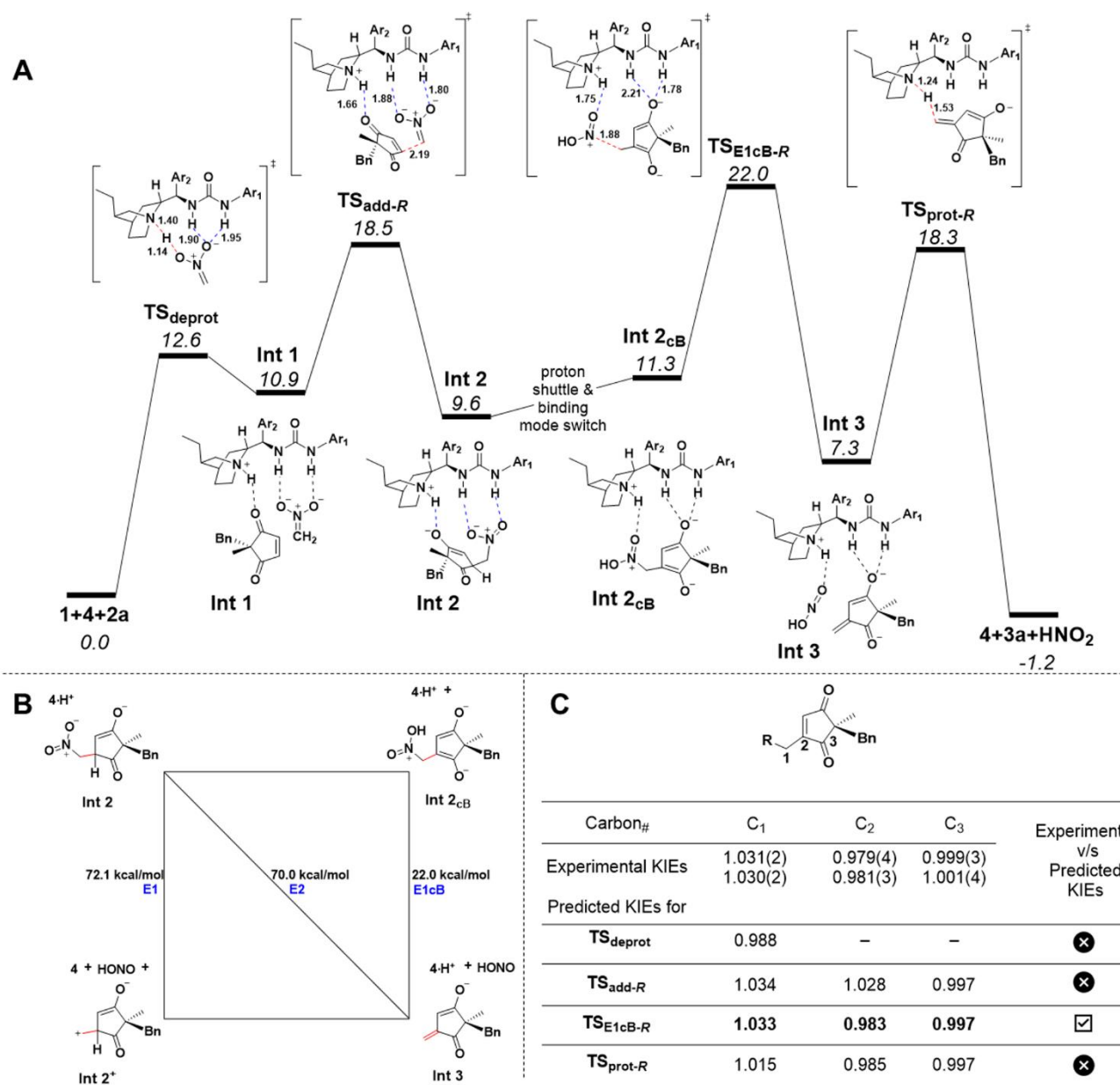
**Figure 2.** (A) The reaction coordinate diagram for the reaction of **1** and **2a** catalyzed by **4** calculated at the M06-2X/6-311+G(d, p) level of theory. All distances are in angstroms (Å). (B) More O' Ferrall–Jencks plot indicating the possible pathways for the conversion of **Int 2** to **Int 3** along with the free energies for the rate-determining step in each pathway. Catalyst structures are omitted for clarity. (C) Comparison of experimental $^{13}C$ KIEs and predicted $^{13}C$ KIEs for each TS along the reaction coordinate. Predictions for $C_2$ and $C_3$ are from TSs shown in 4A whereas predictions for $C_1$ are from analogous TSs utilizing **2b** instead of **2a** as the alkylating agent.

*Predicted KIEs*: The relative free energies of the key intermediates and the TSs for the formation of the major (*R*)-enantiomer **3a** from **1** and **2a** are presented in the full reaction coordinate (Figure 2A). As conjectured from the qualitative interpretation of our experimental KIEs, nitro group elimination is the first irreversible (highest barrier) step in the catalytic cycle for the reaction between **1** and **2a**. To be consistent with the experiments, all predicted KIEs for **1** are from calculations involving **1** and **2a** while predicted KIEs for the nitroalkane are from analogous TSs for **2b** (not shown, see the Supporting Information). Predicted KIEs for

the first irreversible step in the catalytic cycle should be consistent with the experimental KIE values for both **1** and **2b**. To our satisfaction, excellent agreement between all key experimental KIE values and the corresponding predicted values for **TS$_{E1cB-R}$** validate our mechanistic proposal – that nitro elimination via an E1cB pathway is the rate- and enantioselectivity determining step of the reaction. This conclusion is further validated by the mismatch of experimental and predicted KIEs for **1** and **2b** for all other steps in the reaction pathway (Figure 2C).
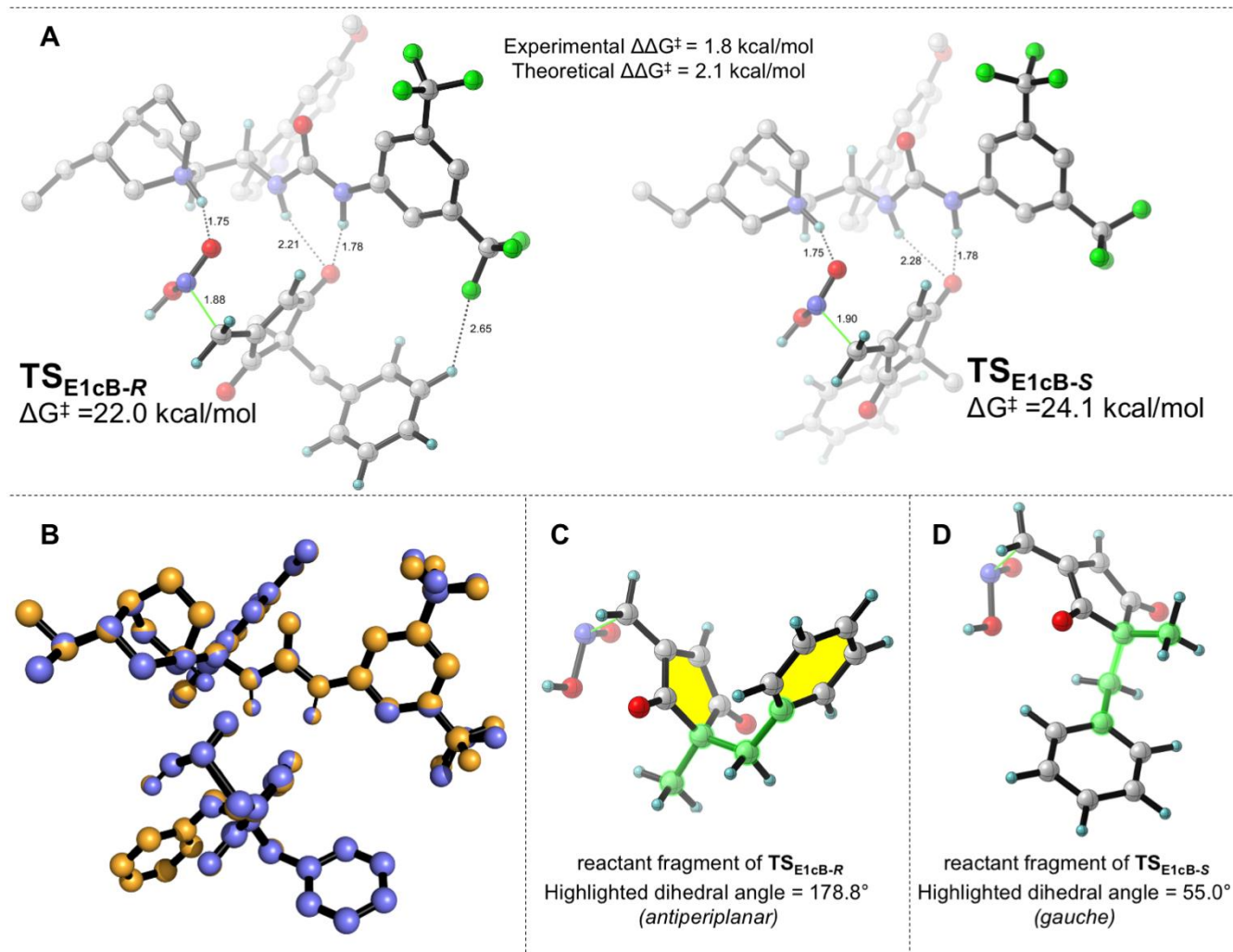
**Figure 3.** (A) Lowest energy transition structures of the enantioselectivity determining step for both enantiomers along with experimental and theoretical free energy barriers. (B) Overlay of the **TS$_{E1cB-R}$** (Blue) and **TS$_{E1cB-S}$** (Orange) demonstrating the significant similarities in the catalyst geometry. (C) Separated reactant fragment of **TS$_{E1cB-R}$** highlighting the π−π interaction (Yellow) and the antiperiplanar orientation of the phenyl and methyl groups. (D) Separated reactant fragment of **TS$_{E1cB-S}$** showing the gauche interaction between the phenyl and the methyl groups of the enedione. Molecular graphics were generated using CYLView.[30]

*Origin of enantioselectivity*: Having established nitrogroup elimination via **TS$_{E1cB-R}$** as the rate- and enantioselectivity-determining step of the reaction, we conducted a detailed conformational search to locate the analogous lowest energy TSs leading to the minor enantiomer of the product [i.e., (*S*)-**3a**]. Our explorations resulted in the identification of **TS$_{E1cB-S}$**, which was found to be 2.1 kcal/mol higher in free energy (ΔΔG$^‡$) than **TS$_{E1cB-R}$** (Figure 3A). This magnitude of ΔΔG$^‡$ corresponds to a predicted er of 98:2 at 263 K, which is in excellent agreement with the experimental er of 97:3 for **3a**. The extent of C−N bond breaking in both the TSs are almost identical (1.88 Å in **TS$_{E1cB-R}$** and 1.90 Å in **TS$_{E1cB-S}$**). Additionally, both **TS$_{E1cB-R}$** and **TS$_{E1cB-S}$** are stabilized by multiple similar H-bonding interactions: The leaving group (HONO) is H-bonded to the protonated quinuclidine (1.75 Å) while the two thiourea NHs are engaged in stabilization of one of the enolate oxygen atoms. In order to maintain these strong stabilizing interactions, the two substituents at the chiral center (Me and Bn) must switch orientations in the two TSs. Consequently, an obvious difference arises – a

moderately stabilizing CH···F interaction (2.65 Å), between one of the aromatic CHs in the benzyl group and one of the CF$_3$ groups in the catalyst, is present only in the TS leading to the major product enantiomer (*R*)-**3a** (**TS$_{E1cB-R}$**).

We performed distortion-interaction/activation-strain analysis[31] (DIAC) to decompose the activation energy into strain energy and interaction energy, and to better understand the origin of selectivity. Strain energy is defined as the energy required to distort the ground state reactants/catalyst into the TS. Interaction energy is defined as the interaction between the distorted catalyst fragment and the reactant fragments in the TS. DIAC decomposed the computed activation energy (ΔΔE$^‡$) of 2.8 kcal/mol into 1.2 kcal/mol of strain energy (ΔΔE$_{strain}^‡$) and 1.6 kcal/mol of interaction energy (ΔΔE$_{int}^‡$) favoring the major enantiomer. Overlaying the catalyst fragment from both TSs (Figure 3B) demonstrates the remarkable conformational similarities between the two low-lying enantiomeric TSs (RMSD 0.01, see the Supporting Information, Figure S26). Careful analysis of the reactant conformations reveals numerous differences in the

reactant geometries (Figure 3C and 3D) that contribute to the observed difference in $\Delta\Delta E_{strain}^{\ddagger}$. Looking down the highlighted C–C bond between the benzylic carbon and the chiral center shows that the phenyl and methyl groups on these adjacent carbon atoms are *anti* to each other in **TS**$_{E1cB-R}$ (Figure 3C) but are *gauche* to each other in **TS**$_{E1cB-S}$ (Figure 3D). The *anti*-orientation in **TS**$_{E1cB-R}$ has the added advantage of stabilizing through CH-π and π-stacking interactions between the phenyl group and the enedione portion of the reactant (yellow highlights Fig 3C). The sterically bulky chiral portion of the catalyst precludes this favorable *anti*-orientation in **TS**$_{E1cB-S}$.

Finally, fragmentation analysis identified key CH⋯F interactions present only in the major enantiomer (*vide supra*). These interactions account for about half of the difference (0.8 kcal/mol) in interaction energies between the competing TSs – demonstrating the importance of the trifluoromethyl groups, not only in modulating the acidity of the urea hydrogens but also in providing a stabilizing electrostatic environment for the TS leading to the major enantiomer. The presence of stronger electrostatic interactions in **TS**$_{E1cB-R}$ (presumably due to shorter urea NH⋯O distance) accounts for the other half of the interaction energy favoring the major enantiomer. Zeroth order symmetry-adapted perturbation theory (SAPT0) calculations performed on the TSs further support this hypothesis. SAPT0 analysis reveals the presence of strong electrostatic interactions (+2.6 kcal/mol) between the catalyst monomer fragment and the reactant monomers favoring **TS**$_{E1cB-R}$. A complete breakdown of SAPT0 interaction energy can be found in the Supporting Information. The analysis presented herein identifies all the key steric and electronic effects contributing to the observed enantioselectivity in this reaction.

## Conclusion

We have used a combination of experimental ^{13}C KIEs and DFT calculations to study the mechanism and the nature of the rate/enantioselectivity-determining step of the bifunctional tertiary aminourea-catalyzed C(sp[2])–H alkylation of cyclopentene-1,3-diones using nitroalkanes as the alkylating agent. Since the chiral center is formed remote from the site of C–H alkylation, understanding of the origin of enantioselectivity is not straightforward. Our studies provide a clear picture of the free energy profile of the reaction and identifies the elimination of the nitro-group as the key step responsible for enantioselectivity in this reaction. Transition state analysis of the enantiomeric TSs identified the key stabilizing interactions as well as conformational effects that dictate the observed enantioselectivity. This information will be critical not only in designing better catalysts for this reaction, but also for the developments of related enantioselective transformations.

## AUTHOR INFORMATION

### Corresponding Author

**Jennifer S. Hirschi –** Department of Chemistry, Binghamton University, Binghamton, New York 13902, United States. **ORCID:** 0000-0002-3470-0561; Email: jhirschi@binghamton.edu

**Santanu Mukherjee –** Department of Organic Chemistry, Indian Institute of Science, Bangalore, India -560012; Email: sm@iisc.ac.in

### Present Addresses

**Rahul Sarkar –** Department of Organic Chemistry, Indian Institute of Science, Bangalore, India -560012;
**Madhu Sudan Manna –** Department of Organic Chemistry, Indian Institute of Science, Bangalore, India -560012;
**Sharath Chandra Mallojjala –** Department of Chemistry, Binghamton University, Binghamton, New York 13902, United States. **ORCID:** 0000-0003-0446-792X.
**Rachel W. Karugu –** Department of Chemistry, Binghamton University, Binghamton, New York 13902, United States.

### Author Contributions

The manuscript was written through contributions of all authors. All authors have given approval to the final version of the manuscript. ‡These authors contributed equally.

## ASSOCIATED CONTENT

This material is available free of charge via the Internet at http://pubs.acs.org."

1.      He, J.; Wasa, M.; Chan, K. S. L.; Shao, Q.; Yu, J. Q., Palladium-Catalyzed Transformations of Alkyl C-H Bonds. *Chem. Rev.* **2017,** *117* (13), 8754-8786.
2.      Lyons, T. W.; Sanford, M. S., Palladium-catalyzed ligand-directed C-H functionalization reactions. *Chem. Rev.* **2010,** *110* (2), 1147-69.
3.      Shi, W.; Liu, C.; Lei, A., Transition-metal catalyzed oxidative cross-coupling reactions to form C-C bonds involving organometallic reagents as nucleophiles. *Chem. Soc. Rev.* **2011,** *40* (5), 2761-76.
4.      Manna, M. S.; Mukherjee, S., Organocatalytic enantioselective formal C(sp(2))-H alkylation. *J. Am. Chem. Soc.* **2015,** *137* (1), 130-3.
5.      DelMonte, A. J.; Haller, J.; Houk, K. N.; Sharpless, K. B.; Singleton, D. A.; Strassner, T.; Thomas, A. A., Experimental and Theoretical Kinetic Isotope Effects for Asymmetric Dihydroxylation. Evidence Supporting a Rate-Limiting "(3 + 2)" Cycloaddition. *J. Am. Chem. Soc.* **1997,** *119* (41), 9907-9908.
6.      Jarvis, C. L.; Hirschi, J. S.; Vetticatt, M. J.; Seidel, D., Catalytic Enantioselective Synthesis of Lactams through Formal [4+2] Cycloaddition of Imines with Homophthalic Anhydride. *Angew. Chem. Int. Ed. Engl.* **2017,** *56* (10), 2670-2674.

7. Wambua, V.; Hirschi, J. S.; Vetticatt, M. J., Rapid Evaluation of the Mechanism of Buchwald–Hartwig Amination and Aldol Reactions Using Intramolecular 13C Kinetic Isotope Effects. *ACS. Catal.* **2020,** *11* (1), 60-67.

8. Singleton, D. A.; Thomas, A. A., High-Precision Simultaneous Determination of Multiple Small Kinetic Isotope Effects at Natural Abundance. *J. Am. Chem. Soc.* **2002,** *117* (36), 9357-9358.

9. The isomerization step also involves this carbon atom; however, protonation steps are typically associated with smaller 13C KIEs that observed experimentally.

10. Singleton, D. A.; Szymanski, M. J., Simultaneous Determination of Intermolecular and Intramolecular13C and2H Kinetic Isotope Effects at Natural Abundance. *J. Am. Chem. Soc.* **1999,** *121* (40), 9455-9456.

11. Becke, A. D., Density-functional thermochemistry. III. The role of exact exchange. *The Journal of Chemical Physics* **1993,** *98* (7), 5648-5652.

12. Grimme, S., Semiempirical GGA-type density functional constructed with a long-range dispersion correction. *J Comput Chem* **2006,** *27* (15), 1787-99.

13. Becke, A., Density-Functional Thermochemistry. V. Systematic Optimization of Exchange-Correlation Functionals. *J. Chem. Phys.* **1997,** *107*, 8554-8560.

14. Weigend, F.; Ahlrichs, R., Balanced basis sets of split valence, triple zeta valence and quadruple zeta valence quality for H to Rn: Design and assessment of accuracy. *Phys. Chem. Chem. Phys.* **2005,** *7*, 3297-3305.

15. Miertus, S.; Scrocco, E.; Tomasi, J., Electrostatic Interaction of a Solute with a Continuum - a Direct Utilization of Abinitio Molecular Potentials for the Prevision of Solvent Effects. *Chem Phys* **1981,** *55* (1), 117-129.

16. Tomasi, J.; Mennucci, B.; Cammi, R., Quantum mechanical continuum solvation models. *Chem. Rev.* **2005,** *105* (8), 2999-3093.

17. Ribeiro, R. F.; Marenich, A. V.; Cramer, C. J.; Truhlar, D. G., Use of solution-phase vibrational frequencies in continuum models for the free energy of solvation. *J. Phys. Chem. B* **2011,** *115* (49), 14556-62.

18. Bigeleisen, J.; Mayer, M. G., Calculation of Equilibrium Constants for Isotopic Exchange Reactions. *J. Chem. Phys.* **1947,** *15* (5), 261-267.

19. Anisimov, V.; Paneth, P., A Program for Studies of Isotope Effects Using Hessian Modifications. *J. Mathem. Chem.* **1999,** *26* (1/3), 75-86.

20. Wigner, E., Crossing of potential thresholds in chemical reactions. *Z. Phys. Chem. B* **1932,** *19*, 203.

21. Zhao, Y.; Truhlar, D. G., The M06 suite of density functionals for main group thermochemistry, thermochemical kinetics, noncovalent interactions, excited states, and transition elements: two new functionals and systematic testing of four M06-class functionals and 12 other functionals. *Theo. Chem. Acc.* **2008,** *120* (1-3), 215-241.

22. Hehre, W. J.; Stewart, R. F.; Pople, J. A., Self-Consistent Molecular-Orbital Methods. I. Use of Gaussian Expansions of Slater-Type Atomic Orbitals. *J. Chem. Phys.* **1969,** *51* (6), 2657-2664.

23. Frisch, M. J.; Trucks, G. W.; Schlegel, H. B.; Scuseria, G. E.; Robb, M. A.; Cheeseman, J. R.; Scalmani, G.; Barone, V.; Petersson, G. A.; Nakatsuji, H.; Li, X.; Caricato, M.; Marenich, A. V.; Bloino, J.; Janesko, B. G.; Gomperts, R.; Mennucci, B.; Hratchian, H. P.; Ortiz, J. V.; Izmaylov, A. F.; Sonnenberg, J. L.; Williams; Ding, F.; Lipparini, F.; Egidi, F.; Goings, J.; Peng, B.; Petrone, A.; Henderson, T.; Ranasinghe, D.; Zakrzewski, V. G.; Gao, J.; Rega, N.; Zheng, G.; Liang, W.; Hada, M.; Ehara, M.; Toyota, K.; Fukuda, R.; Hasegawa, J.; Ishida, M.; Nakajima, T.; Honda, Y.; Kitao, O.; Nakai, H.; Vreven, T.; Throssell, K.; Montgomery Jr., J. A.; Peralta, J. E.; Ogliaro, F.; Bearpark, M. J.; Heyd, J. J.; Brothers, E. N.; Kudin, K. N.; Staroverov, V. N.; Keith, T. A.; Kobayashi, R.; Normand, J.; Raghavachari, K.; Rendell, A. P.; Burant, J. C.; Iyengar, S. S.; Tomasi, J.; Cossi, M.; Millam, J. M.; Klene, M.; Adamo, C.; Cammi, R.; Ochterski, J. W.; Martin, R. L.; Morokuma, K.; Farkas, O.; Foresman, J. B.; Fox, D. J. *Gaussian 16 Rev. C.01*, Wallingford, CT, 2016.

24. Jeziorski, B.; Moszynski, R.; Szalewicz, K., Perturbation-Theory Approach to Intermolecular Potential-Energy Surfaces of Van-Der-Waals Complexes. *Chem. Rev.* **1994,** *94* (7), 1887-1930.

25. Szalewicz, K., Symmetry-adapted perturbation theory of intermolecular forces. *WIREs Comput. Mol. Sci.* **2012,** *2* (2), 254-272.

26. Hohenstein, E. G.; Sherrill, C. D., Density fitting of intramonomer correlation effects in symmetry-adapted perturbation theory. *J. Chem. Phys.* **2010,** *133* (1), 014101.

27. Hohenstein, E. G.; Sherrill, C. D., Density fitting and Cholesky decomposition approximations in symmetry-adapted perturbation theory: Implementation and application to probe the nature of pi-pi interactions in linear acenes. *J. Chem. Phys.* **2010,** *132* (18), 184111.

28. Turney, J. M.; Simmonett, A. C.; Parrish, R. M.; Hohenstein, E. G.; Evangelista, F. A.; Fermann, J. T.; Mintz, B. J.; Burns, L. A.; Wilke, J. J.; Abrams, M. L.; Russ, N. J.; Leininger, M. L.; Janssen, C. L.; Seidl, E. T.; Allen, W. D.; Schaefer, H. F.; King, R. A.; Valeev, E. F.; Sherrill, C. D.; Crawford, T. D., PSI4: an open-source ab initio electronic structure program. *WIREs Comput. Mol. Sci.* **2012,** *2* (4), 556-565.

29. The estimated half life based on Gibbs-Eyring equation for a free energy barrier of 21.5 kcal/mol for a unimolecular reaction at 263K with a transmission coefficient of 1 is 1.07 days. The reported reaction takes about 48 hours for completion.

30. Legault, C. Y. *CYLview, 1.0b; Université de Sherbrooke, 2009 (http://www.cylview.org)*.

31. Bickelhaupt, F. M.; Houk, K. N., Analyzing Reaction Rates with the Distortion/Interaction-Activation Strain Model. *Angew. Chem. Int. Ed. Engl.* **2017,** *56* (34), 10070-10086.

**Entry for Table of Contents**